Progress In Electromagnetics Research C, Vol. 83, 195–203, 2018

Accurate Design of Deep Sub-Wavelength Metamaterials for Wireless Power Transfer Enhancement

Chunyu Zhao*, [1] , Senlin Zhu[1] , Hui Zhu[1] , Zhenyu Huang[1] , and Xudong Luo[2]

Abstract—Deep sub-wavelength metamaterials for a wireless power transfer system (WPT) is still a challenge in design and optimization. We propose a large capacitor spiral metamaterial (LCSM) which involves inherent advantages of low operating frequencies and compact structures. The ratio of electromagnetic wavelength to the metamaterial scale can easily reach 1000 at the operation frequency of several megahertz. A hybrid search method, which combines a modified simulated annealing algorithm and a differential evolution algorithm, is applied to the accurate and automatic design of LCSM. The permeability of LCSM is evaluated by finite element analysis and then verified by experimental results. Finally, a small-size WPT system working at 6.78 MHz was constructed to evaluate LCSM. The results show that LCSM can enhance the transfer efficiency of the WPT system from 5.54% to 22.40% at a transmission distance of 15 cm.

1. INTRODUCTION

Wireless power transfer (WPT) system technology has continuously attracted lots of attention for a hundred years. Since Tesla demonstrated the possibility of WPT via electromagnetic field in 1905 [1], many researchers have devoted a lot of effort to improve the WPT performance for different applications. However, limitations of the current WPT system, especially in transmission distance, efficiency, and power capacity, restrict applications in wide fields [2, 3]. In 2007, Soljacic and his group designed a couple of self-resonant and high-quality coils to achieve strong effects of the resonant coupling that enhanced WPT up to 60 watts with 40% efficiency over a distance of 2 meters [4]. However, as the size of self-resonant coils is so large, strong magnetic resonant coupling is difficult to realize in portable devices. Alternatively, by inserting metamaterials with the negative permeability (μ), the coupling between the transmit and receive coils becomes stronger, and consequently, the transmission energy and efficiency can be enhanced. This phenomenon was firstly explored by Wang et al. in simulations [5] then verified by Urzhumov and Smith in theories [6], and consequently investigated by numerous experimental works [7–10].

In consideration of safety, operating frequencies of a WPT system are usually restrained in tens of megahertz or even lower [11]. For example, 6.78 MHz is widely adopted as the center frequency in the ISM band. For portable devices, the wireless power transfer technology requires metamaterials as small as in decimeter scale. Thus, the ratio of the electromagnetic wavelength (λ) to metamaterial scale (s) must reach up to 100 (λ_0/s), known as deep sub-wavelength metamaterial. Chen et al. presented a highly subwavelength magnetic metamaterial consisting of independent planar spiral elements, and its λ_0/s reaches 700 [12]. And Rodrí guez developed a kind of compact low-frequency metamaterial using

Received 25 January 2018, Accepted 4 April 2018, Scheduled 23 April 2018

* Corresponding author: Chunyu Zhao (zhaocy@sjtu.edu.cn).

[1] Department of Instrument Science and Engineering, School of Electronic Information and Electrical Engineering, and Shanghai Engineering Research Center for Intelligent Diagnosis and Treatment Instrument, Shanghai Jiao Tong University, Shanghai 200240, China. [2] School of Physics and Astronomy, Key Laboratory of Artificial Structures and Quantum Control (Ministry of Education), and National Demonstration Center for Experimental Physics Education, Shanghai Jiao Tong University, Shanghai 200240, China.

ferrite loaded solenoid, and its λ_0/s is about 6277 [10]. However, this metamaterial is difficult to apply in practice due to the complex structure with external capacitors.

As deep sub-wavelength metamaterials normally possess much more complex structures than those working at GHz and above, the accurate design of the deep sub-wavelength metamaterials is a difficult and time-consuming task. Thus, a machine-based automation design methodology is required to optimize metamaterials for different WPT systems. Although some automation design methods, such as topology optimization method [13] and heuristic optimization method [14], are successfully adopted to design and optimize metamaterials in GHz, the accurate design of deep sub-wavelength metamaterials in MHz still requires to be investigated.

This paper introduces a kind of highly sub-wavelength metamaterials with the negative permeability at the ISM band, e.g., the center frequency at 6.78 MHz. Based on the sensitivity analysis of the parameters on this metamaterial, a hybrid search method is then developed to design and optimize the metamaterial with high precision. A WPT system was fabricated to validate the enhanced performance of this metamaterial in the energy transfer efficiency.

2. DESIGN OF DEEP SUB-WAVELENGTH METAMATERIALS

In order to realize a compact metamaterial with negative permeabilities at MHz, we propose a large capacitor spiral metamaterial (LCSM), as shown in Fig. 1. The structure of LCSM consists of dual-layer square spiral copper wires etching on both sides of the substrate slab. The square spiral copper wires are different from the planar spiral copper wires introduced in [12]. Here, the width of the inner wire rings is narrow, while the width of the outer-most ring is obviously wider. The copper wires on dual layers are connected through the vias at the end of the spiral inner rings. Specifically, the length and thickness of the unit cell are denoted as s and d, respectively. The length and width of the outer wire ring are denoted as h and b, respectively, and the width of the inner rings is denoted as w. g denotes the width of the wire clearance, and n denotes the number of turns of the spiral.

The unit cell of LCS can be equivalently represented by a simple circuit model, as shown in Fig. 2. And the resonant frequency f_0 can be evaluated by

$$f_0 = \frac{1}{2\pi\sqrt{(L_1 + L_2)(C_1 + C_2)}} \tag{1}$$

where L_1 and L_2 are equivalent inductances of the front and back spirals, respectively, and C_1 and C_2 arise from the inner rings and outer-most ring of the two-layer copper wires, respectively. In order to achieve a lower resonant frequency, L_1 and L_2 are connected in series through vias to produce a greater inductance. In the alternating electromagnetic field, the inductive charge flows through L_1 and L_2, and then the positive and negative charges are gathered in the two outer-most rings on the two layers, respectively. Therefore, the width of the outmost ring is set to be wide to produce an effective capacitor C_2 as large as possible in a compact size. C_1 and C_2 are connected in parallel to produce a greater capacity.

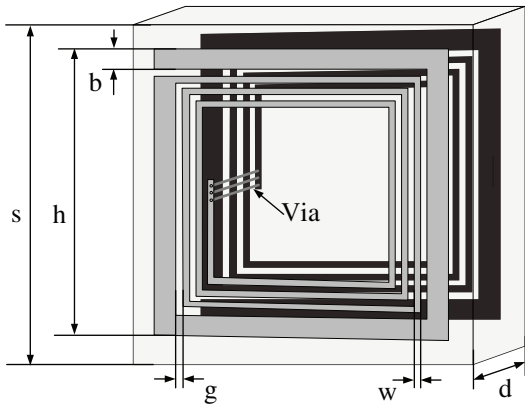

Figure 1. Schematic 3D view of the LCSM unit cell.

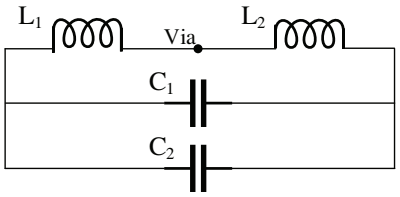

Figure 2. Equivalent circuit model of the LCSM unit cell.

LCSM is able to make larger inductance and capacitance under the same size of unit cell, which means a lower resonant frequency. Hence, LCSM has the advantages of low operating frequencies and compact structure, whose λ_0/s is about 1000.

3. OPTIMIZATION OF LCSM USING A HYBRID SEARCH ALGORITHM

For a metamaterial applied to a WPT system, the operating frequency and permeability of the metamaterials are the most important factors determining whether the metamaterial can effectively work in a certain WPT system or not. The operating frequency (f) and resonant frequency of metamaterials are not the same. The equivalent permeability of the metamaterials is negative at the operating frequency. The equivalent permeability curve with respect to the frequency is stable around the operating frequency and sharp around the resonant frequency. Usually, the operating frequency is a little greater than resonant frequency. The real part of permeability (μ') is usually designed to be a required negative value to enhance the efficiency of the power transfer. Meanwhile, the imaginary part (μ'') is desired to be as small as possible, since the imaginary part determines the absorption of the electromagnetic waves. This also means maximizing the quality factor of the resonant material coil. Parameters h, n, d, g, w, and b are chosen to design LCSM, which affect the equivalent capacitance and inductance of the metamaterial unit to varying degrees. In addition, these six parameters can be adjusted independently. Therefore, an objective function is fabricated as

$$\begin{aligned} &\text{Objective:} \\ &\qquad \text{Min}\{\alpha(\mu^{'} - \mu_{\text{t}}^{'})^2 + \beta(\mu^{''})^2\} \mid_{\text{f=f}_{\text{t}}} \\ &\text{Constrains:} \\ &\qquad n_{\min} \le n \le n_{\max}, \quad h_{\min} \le h \le h_{\max}, \\ &\qquad b_{\min} \le b \le b_{\max}, \quad d_{\min} \le d \le d_{\max}, \\ &\qquad g_{\min} \le g \le g_{\max}, \quad w_{\min} \le w \le w_{\max}, \end{aligned} \tag{2}$$

where α and β are the user defined weights of the real and imaginary parts of the permeability, respectively. All the variables are normalized by linear normalization. f is the operating frequency of LCSM, f_t the target operating frequency, and μ_t the target real part of permeability. The constraints of parameters are defined by user, according to the fabrication limitations, application requirements and other special demands.

First, the relationships of the operating frequency and the six parameters were investigated, as shown in Fig. 3. These six independent parameters determine the objective function together. The control variable method was used to make parameters sensitivity analysis. The other parameters were in the middle of the range of values when one parameter changes. A finite element model was used to calculate the objective function based on a set of parameters with specific values. According to their sensitivities to the operating frequency, those parameters were divided into high-sensitive parameters (HSPs: n, h, d) and low-sensitive parameters (LSPs: w, g, b). Thus,correspondingly the design process was mainly divided into two steps, i.e., the general design to get HSPs firstly and the elaborate design to get LSPs. In the general design, we employ a modified simulated annealing (MSA) algorithm to optimize HSPs rapidly [15]. After that, the results were very close to the target. Hence, in the elaborate design a differential evolution (DE) algorithm [16] was used to determine LSPs accurately and stably. The overall flow of the algorithm is presented in Fig. 4.

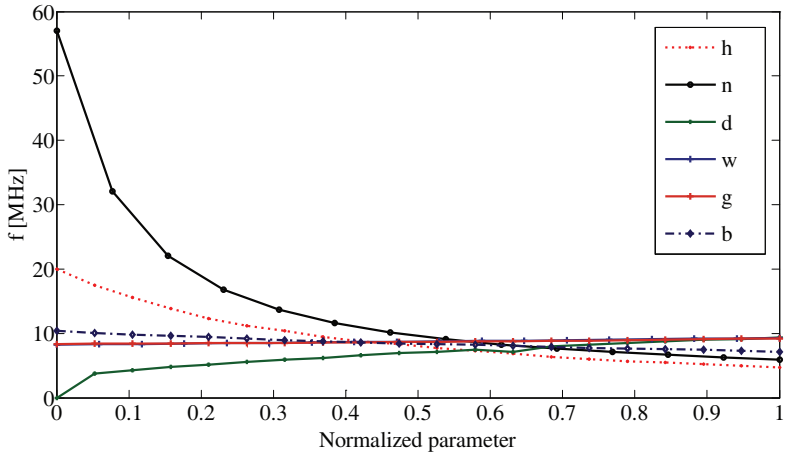

Figure 3. Relationship between the operating frequency and each parameter.

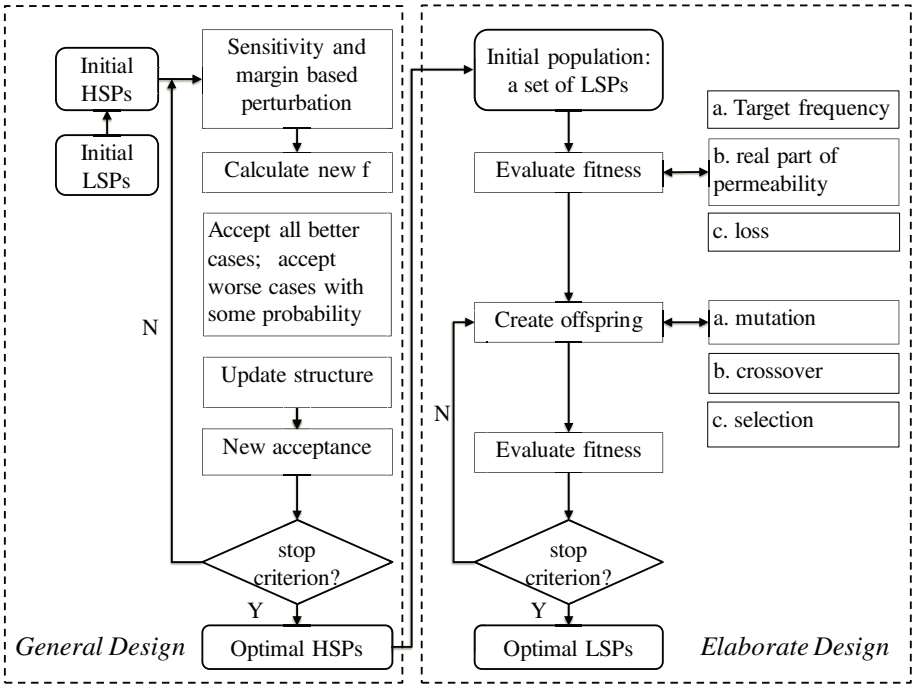

Figure 4. Algorithm flow of the hybrid method with MSA and DE.

3.1. General Design: MSA

Initially, the parameters were chosen randomly in the permissible range. The process of simulated annealing requires a perturbation in each iteration. The better case is always accepted while the worse case is accepted with some probability. The probability decreases according to some schedules after each iteration [17]. Only the operating frequency is concerned in the general design. When the error between operating frequency and the target frequency is less than 5%, the general design stops. All HSPs are monotonous, and then the perturbation of those parameters has directivity. The modification of each parameter in each perturbation is shown as (3)

$$\begin{aligned} n &= n_0 + rate_n \cdot step_n \cdot \Delta f \\ h &= h_0 + rate_h \cdot step_h \cdot \Delta f \\ d &= d_0 + rate_d \cdot step_d \cdot \Delta f \end{aligned} \tag{3}$$

where $\Delta f = f - f_t$ represents the difference of the current operating frequency and the target operating frequency. n_0, h_0, and d_0 are the geometrical parameters before the perturbation. $rate_n$, $rate_h$, and $rate_d$ represent the weight of n, h, and d, respectively. The sum of those *rate* is 1. The parameter farther away from the boundary of its ranges is assigned a greater *rate*. $step_n$, $step_h$, and $step_d$ are the sensitivities of n, h, and d, respectively. *step* indicates the change of each parameter corresponding to 1 Hz change of operating frequency. In each iteration, if the symbol of Δf changes, *step* decreases. Otherwise, *step* increases. The strategy takes margin and sensitivity of each parameter into consideration so that each parameter finds a moderate target more quickly.

3.2. Elaborate Design: DE

Attributing to the former general design, the search space became much smaller. All the factors in the objective function are taken into consideration in the elaborate design. The DE algorithm starts with an initial population with a set of candidate solutions, which are chosen randomly. In each iteration of DE, the offspring are generated by mutation, crossover and selection from the original solutions in the population. The offspring solution replaces the original solution if improvement occurs. Otherwise, the original one remains, and the population is updated. Then the best solution in the population is selected and evaluated. When the precision requirement is satisfied, or the process reaches a certain number of iterations, the procedure stops, and the final solution is achieved.

Table 1. Structural parameters of the simulated and manufactured LCSM unit cell.

	s [mm]	h [mm]	n [turns]	d [mm]	w [mm]	g [ww]	b [mm]
Simulated	49.50	44.8696	10	1.00	0.6002	0.4701	2.5498
Manufactured	49.50	44.87	10	1.00	0.60	0.47	2.44

After the general design and elaborate design, the optimized parameters were obtained as listed in Table 1. Taking into account the actual machining accuracy, we revised the value to 0.01 level in the fabricated model. In this sample, we set the target permeability of LCSM as -0.8. The designed metamaterial achieved a negative permeability of $-0.8201 + 0.2780i$ at 6.78 MHz. It is demonstrated that this method only has an error of 2.51% in the real part of the permeability. Besides, the imaginary part of the permeability is 0.2780, which shows a certain degree of the dielectric loss.

4. EXPERIMENT AND RESULTS

4.1. Measurement of LCSM Unit Cell

The measurement rig of permeability for a LCSM unit cell is shown as Fig. 5. $Coil_T$ and $Coil_R$ were single circle square copper coils of 52 mm in size, printed on an FR4 circuit board, as shown in Fig. 5(a). They were placed 1.8 centimeters apart in parallel. The energy input into $Coil_T$ produces a changing electromagnetic field. In this electromagnetic field, $Coil_R$ can receive inductive energy and generate induction electromotive force. The enhancement of induced electromotive force caused by LCSM insertion is proportional to the equivalent μ of LCSM [18]. A vector network analyzer (VNA), Agilent E5071C, was used to test transmission parameters $S21$. $Coil_T$ and $Coil_R$ were connected to $Prot_T$ and $Port_R$ of the VNA, respectively. The equivalent permeability of LCSM cells can be calculated simply by

$$\mu = \frac{S21_{LCSM}}{S21_{no\_LCSM}} \tag{4}$$

The simulated and measured permeabilities of the LCSM unit cell were compared, as shown in Fig. 6. μ' is shown in Fig. 6(a) while μ'' is shown in Fig. 6(b). The equivalent permeability of LCSM in the finite element model was calculated by an improved S-parameter retrieval method which was introduced in [19]. The simulation results of resonant frequency of the LCSM unit cell are in good

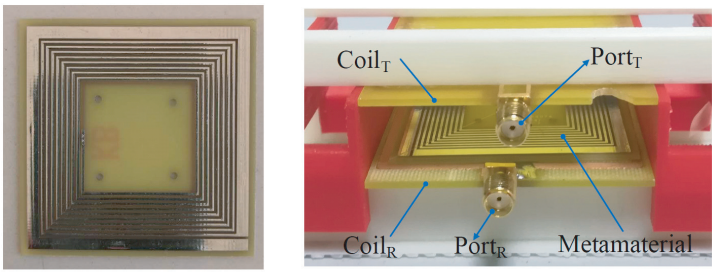

(a) LCSM cell (b) Measurement device

Figure 5. Measurement rig of permeability for the LCSM unit cell.

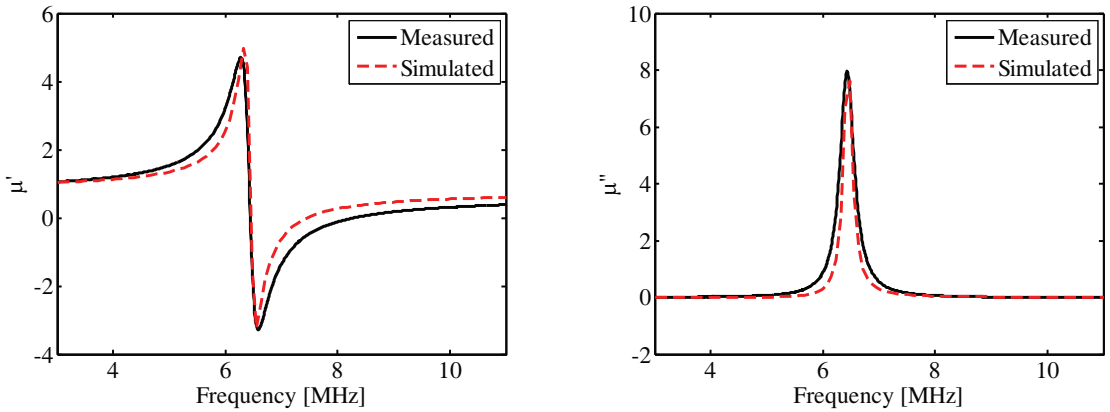

(a) Real part of permeability (b) Imaginary part of permeability

Figure 6. Simulated and measured permeability of the LCSM unit cell.

correspondence with the experimental results. The difference of the real and imaginary parts of the permeability between the experimental and the simulated results mainly comes from the difference of the derivation of the permeability. Due to the precision limitation of the experimental rig, the method of calculating the permeability in the experiment obtains an approximate result. The results show that the proposed LCSM model can obtain accurate resonant frequencies and acceptable permeability values.

4.2. WPT System with LCSM

The schematic diagram of the WPT system with LCSM is shown in Fig. 7. This experimental system includes two resonant coils and an LCSM slab. L_T and L_R are inductors of the transmit and receive coils, respectively. These two coils were both made up of a 4-turn wire, and the diameter of the wire is 1.1 mm. Their radii were r_1 and r_2, respectively. The distance between them was D_1. Two capacitors (C_T and C_R) were used to tune the resonant frequency of the system to fit LCSM. The distance between the transmit coil and LCSM was D_2. V_S is the power source of the WPT system, and R_L is the load. In this case, D_1 was 15 cm; r_1 and r_2 were both 7 cm; D_2 was variable.

A photograph of the WPT system is shown in Fig. 8. LCSM was made up of 4×4 array cells with a size of 20 cm×20 cm, as shown in Fig. 8(a). A VNA, Agilent E5071C, was used as the power source and the load. Thus the source impedance and load impedance were both 50 Ω. The self-inductance and resistance of coils were measured by an HP4192A LCR meter. L_T and L_R were both 5.15 uH, and their resistances were both 0.39 Ω at 6.78 MHz. In order to set the resonant frequency of the WPT system to 6.78 MHz, C_T and C_R were adjusted to approximately 107 pF.

The measured efficiency of the WPT system is shown in Fig. 9. It should be noted that the efficiency is calculated by square of $|S_{21}|$. The black line in the figure shows that the WPT system resonates at 6.78 MHz, with a maximum transmission efficiency of 5.54%. The red line in the figure shows the effect

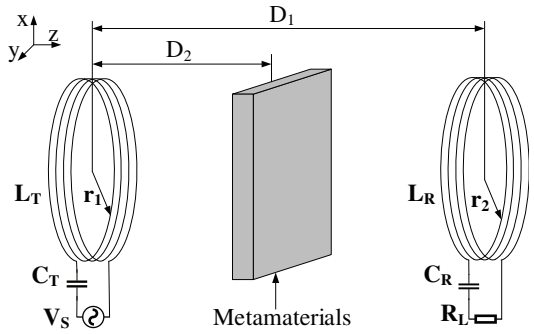

Figure 7. Schematic diagram of the WPT system with meatmaterials.

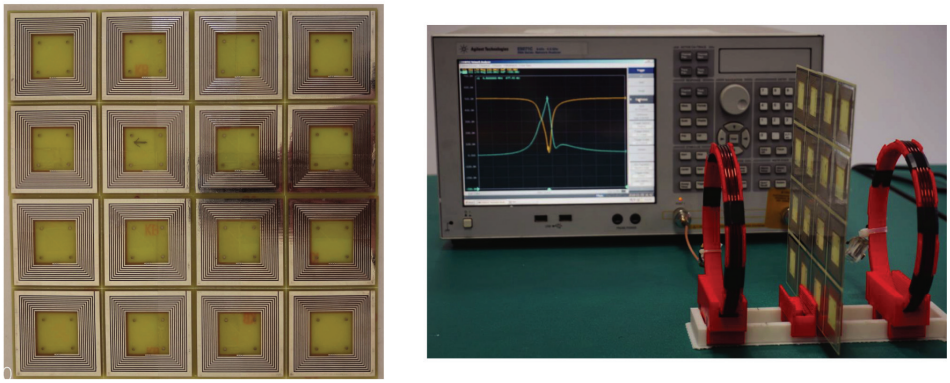

(a) LCSM 4×4 cell (b) WPT system with LCSM

Figure 8. Photographs of the experimental setup.

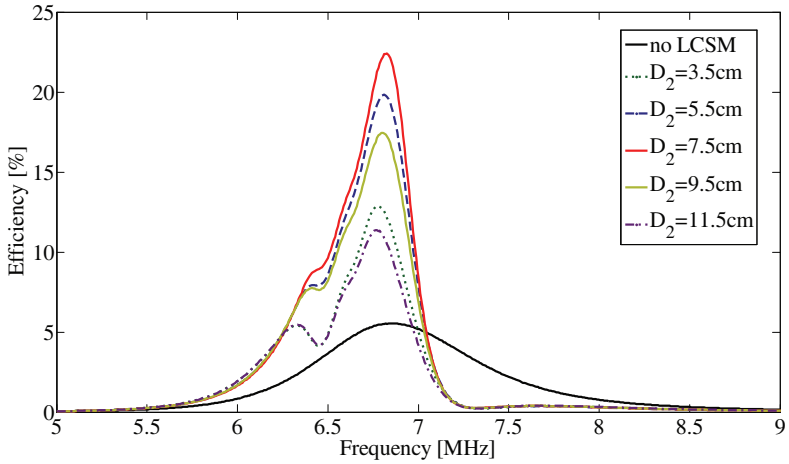

Figure 9. Measured transmission efficiency of the WPT system.

of LCSM on the transmission performance of the WPT system. When the LCSM was placed in the middle ($D_2 = 7.5\,\text{cm}$) of the WPT system, the transmission efficiency was increased to 22.40%. The above experimental results show that LCSM has significant effects on the performance of the WPT system. In addition, in order to evaluate the effects of different placement positions of LCSM, a group of comparative experiments were carried out by setting the value of D_2 as 3.5 cm, 5.5 cm, 9.5 cm and

11.5 cm. Accordingly, their maximum transmission efficiency values are 12.86%, 19.84%, 17.44% and 11.38%, respectively. Based on the above experimental data, we can find that when LCSM is placed at the center of the coils, the transmission efficiency reaches the maximum value. When the metamaterial is in an off-center position, the transmission efficiency of the WPT system decreases. Moreover, when the LCSM deviates from the same distance to the transmit coil and receive coil, the WPT performance of the former is a bit better.

5. CONCLUSION

In this paper, we propose a kind of high sub-wavelength negative permeability index metamaterials which has a large capacitor spiral structure. This kind of structure is easy to realize low resonant frequencies at compact size of metamaterial cells. A hybrid search method is used to design and optimize LCSM, which guarantees high precision and reasonable design time. The designed LCSM works at 6.78 MHz with the cell size of 49 mm, realizing λ_0/s of 903. LCSM was evaluated by FEA and experiment results, and the results agree well. Experimental results verify that the WPT system integrating with metamaterials can improve the energy transfer efficiency significantly. The energy transfer efficiency of the WPT increases from 5.5% to 22.4% by inserting an LCSM plate of 4 × 4 cell cells in the middle of the transmitting coil and the receiving coil 15 cm apart.

REFERENCES

1. Tesla, N., "The transmission of electrical energy without wires as a means for furthering peace," *Electrical World & Engineer*, 1905.
2. Kalwar, K. A., M. Aamir, and S. Mekhilef, "Inductively coupled power transfer (ICPT) for electric vehicle charging — A review," *Renewable & Sustainable Energy Reviews*, Vol. 47, 462–475, 2015.
3. Barman, S. D., A. W. Reza, N. Kumar, M. E. Karim, and A. B. Munir, "Wireless powering by magnetic resonant coupling: Recent trends in wireless power transfer system and its applications," *Renewable & Sustainable Energy Reviews*, Vol. 51, 1525–1552, 2015.
4. Kurs, A., A. Karalis, R. Moffatt, J. D. Joannopoulos, P. Fisher, and M. Soljacic, "Wireless power transfer via strongly coupled magnetic resonances," *Science*, Vol. 317, No. 5834, 83, 2007.
5. Wang, B., T. Nishino, and K. H. Teo, "Wireless power transmission efficiency enhancement with metamaterials," *in IEEE International Conference on Wireless Information Technology and Systems*, 1–4, 2010.
6. Urzhumov, Y. and D. R. Smith, "Metamaterial-enhanced coupling between magnetic dipoles for efficient wireless power transfer," *Physical Review B*, Vol. 83, No. 20, 99–105, 2011.
7. Choi, J. and C. H. Seo, "High-efficiency wireless energy transmission using magnetic resonance based on negative refractive index metamaterial," *Progress in Electromagnetics Research*, Vol. 106, 33–47, 2010.
8. Wang, B., K. H. Teo, T. Nishino, W. Yerazunis, J. Barnwell, and J. Zhang, "Experiments on wireless power transfer with metamaterials," *Applied Physics Letters*, Vol. 98, No. 25, 254101, 2011.
9. Ranaweera, A. L. A. K., T. P. Duong, and J. W. Lee, "Experimental investigation of compact metamaterial for high efficiency mid-range wireless power transfer applications," *Journal of Applied Physics*, Vol. 116, No. 4, 83–86, 2014.
10. Rodríguez, E. S. G., A. K. Ramrakhyani, D. Schurig, and G. Lazzi, "Compact low-frequency metamaterial design for wireless power transfer efficiency enhancement," *IEEE Transactions on Microwave Theory & Techniques*, Vol. 64, No. 5, 1644–1654, 2016.
11. Engineers, E. E. and I. S. Board, "Ieee standard for safety levels with respect to human exposure to radio frequency electromagnetic fields, 3 KHz to 300 GHz," *IEEE Std. C.*, 1, 2002.
12. Chen, W. C., C. M. Bingham, K. M. Mak, N. W. Caira, and W. J. Padilla, "Extremely sub-wavelength planar magnetic metamaterials," *Physical Review B*, Vol. 85, No. 20, 1614–1621, 2012.

13. Zhou, S., W. Li, G. Sun, and Q. Li, "A level-set procedure for the design of electromagnetic metamaterials," *Optics Express*, Vol. 18, No. 7, 6693, 2010.
14. Chen, P. Y., C. H. Chen, H. Wang, J. H. Tsai, and W. X. Ni, "Synthesis design of artificial magnetic metamaterials using a genetic algorithm," *Optics Express*, Vol. 16, No. 17, 12806, 2008.
15. Zhu, H., X. Luo, C. Zhao, Z. Hong, and Z. Huang, "Design and optimization of deep sub-wavelength metamaterials using a hybrid search algorithm," *in Wireless Power Transfer Conference*, 2017.
16. Storn, R. and K. Price, "Differential evolution — A simple and efficient heuristic for global optimization over continuous spaces," *Journal of Global Optimization*, Vol. 11, No. 4, 341–359, 1997.
17. Kirkpatrick, S., C. D. Gelatt, Jr., and M. P. Vecchi, "Optimization by simulated annealing," *Readings in Computer Vision*, Vol. 220, No. 4598, 606–615, 1983.
18. Wu, Q., Y. H. Li, N. Gao, F. Yang, Y. Q. Chen, K. Fang, Y. W. Zhang, and H. Chen, "Wireless power transfer based on magnetic metamaterials consisting of assembled ultra-subwavelength meta-atoms," *EPL*, Vol. 109, No. 6, 2015.
19. Smith, D. R., D. C. Vier, T. Koschny, and C. M. Soukoulis, "Electromagnetic parameter retrieval from inhomogeneous metamaterials," *Physical Review E Statistical Nonlinear & Soft Matter Physics*, Vol. 71, No. 3, Pt. 2B, 036617, 2005.